Publications   **Bioengineering**

1-2013

Predictive modeling of the virtual Hemi-Fontan operation for second stage single ventricle palliation: Two patient-specific cases

Ethan Kung

Alessia Baretta

Catriona Baker

Gregory Arbia

Giovanni Biglino

See next page for additional authors

Authors

Ethan Kung, Alessia Baretta, Catriona Baker, Gregory Arbia, Giovanni Biglino, Chiara Corsini, Silvia Schievano, Irene E. Vignon-Clementel, Gabriele Dubini, Giancarlo Pennati, Andrew Taylor, Adam Dorfman, Anthony M. Hlavacek, Alison L. Marsden, Tain-Yen Hsia, and Francesco Migliavacca

Predictive modeling of the virtual Hemi-Fontan operation for second stage single ventricle palliation: two patient-specific cases

Ethan Kung[1], Alessia Baretta[2], Catriona Baker[3], Gregory Arbia[4], Giovanni Biglino[3], Chiara Corsini[2], Silvia Schievano[3], Irene E. Vignon-Clementel[4], Gabriele Dubini[2], Giancarlo Pennati[2], Andrew Taylor[3], Adam Dorfman[5], Anthony M Hlavacek[6], Alison L. Marsden[1], Tain-Yen Hsia[3], Francesco Migliavacca[2]
for the Modeling Of Congenital Hearts Alliance (MOCHA)+ Investigators

1. Mechanical and Aerospace Engineering Department, University of California San Diego, San Diego, CA, USA

2. Laboratory of Biological Structure Mechanics, Structural Engineering Department, Politecnico di Milano, Italy

3. Cardiorespiratory Unit, Great Ormond Street Hospital for Children and UCL Institute of Cardiovascular Science, London, UK

4. INRIA, Paris-Rocquencourt, Le Chesnay, France

5. Division of Pediatric Cardiology, Department of Pediatrics, University of Michigan Medical School, Ann Arbor, MI, USA

6. Division of Pediatric Cardiology, Department of Pediatrics, Medical University of South Carolina, Charleston, South Carolina 29425, USA

Corresponding Author:
Francesco Migliavacca
Laboratory of Biological Structure Mechanics
Structural Engineering Department
Politecnico di Milano,
Piazza Leonardo da Vinci, 32
20133 Milano, Italy
Tel: +39.02.2399.4316
Fax: +39.02.2399.4286
francesco.migliavacca@polimi.it

Article type: Original Contribution

Keywords: Single-ventricle, Fontan, multi-scale modeling, CFD, Hemi-Fontan, patient specific modeling

ABSTRACT

Single ventricle hearts are congenital cardiovascular defects in which the heart has only one functional pumping chamber. The treatment for these conditions typically requires a three-staged operative process where Stage 1 is typically achieved by a shunt between the systemic and pulmonary arteries, and Stage 2 by connecting the superior venous return to the pulmonary circulation. Surgically, the Stage 2 circulation can be achieved through a procedure called the Hemi-Fontan, which reconstructs the right atrium and pulmonary artery to allow for an enlarged confluence with the superior vena cava.

Based on pre-operative data obtained from two patients prior to Stage 2 surgery, we developed two patient-specific multi-scale computational models, each including the 3D geometrical model of the surgical junction constructed from magnetic resonance imaging, and a closed-loop systemic lumped-parameter network derived from clinical measurements. "Virtual" Hemi-Fontan surgery was performed on the 3D model with guidance from clinical surgeons, and a corresponding multi-scale simulation predicts the patient's post-operative hemodynamic and physiologic conditions. For each patient, a post-operative active scenario with an increase in the heart rate (HR) and a decrease in the pulmonary and systemic vascular resistance (PVR and SVR) was also performed. Results between the baseline and this 'active' state were compared to evaluate the hemodynamic and physiologic implications of changing conditions.

Simulation results revealed a characteristic swirling vortex in the Hemi-Fontan in both patients, with flow hugging the wall along the SVC to Hemi-Fontan confluence. One patient model had higher levels of swirling, recirculation, and flow stagnation. However, in both models, the power loss within the surgical junction was less than 13% of the total power loss in the pulmonary circulation, and less than 2% of the total ventricular power. This implies little impact of the surgical junction geometry on the SVC pressure, cardiac output, and other systemic parameters. In contrast, varying HR, PVR, and SVR led to significant changes in theses clinically relevant global parameters.

Adopting a work-flow of customized virtual planning of the Hemi-Fontan procedure with patient-specific data, this study demonstrates the ability of multi-scale modeling to reproduce patient specific flow conditions under differing physiological states. Results demonstrate that the same operation performed in two different patients can lead to different hemodynamic characteristics, and that modeling can be used to uncover physiologic changes associated with different clinical conditions.

INTRODUCTION

Single ventricle physiology, in which the infant has only one functional pumping chamber, is one of the most severe forms of congenital heart disease. Without intervention, the condition is not compatible with life, requiring immediate surgical treatment after birth, followed by two additional surgeries within the first few years of life. The surgeries are staged such that at each stage the circulation provides adequate systemic oxygen delivery without severe, long-term volume overloading of the ventricle. The final goal is to bypass the heart by connecting the entire systemic venous return directly to the pulmonary arterial system, resulting in an in-series circulation driven by a single ventricle(1).

The Stage 1 surgery is performed within the first few days of life, with the patency of the ductus arteriosus ensured by infusion of prostaglandin E2 until the operation. In most cases a systemic-to-pulmonary shunt (Fig. 1a) provides balanced flow to the pulmonary circulation while maintaining an unrestricted aortic outflow and systemic venous return. The stage 2 surgery is performed at about 6 months of age, after the pulmonary vascular resistance has decreased due to lung growth (2). The surgery removes the systemic-to-pulmonary shunt, or disconnects the pulmonary artery from the systemic arterial circulation (depending on stage 1 anatomy), and attaches the superior vena cava (SVC) to the pulmonary artery to provide pulmonary flow. After a few years of age as the proportion of systemic venous return from the lower body increases, the stage 3 surgery, the Fontan procedure, is performed, during which the inferior vena cava (IVC) is also connected to the pulmonary artery, completing the conversion to single ventricle circulation.

The transition from Stage 1 to Stage 2 circulation is particularly important as the single ventricle is relieved of the workload of providing pulmonary blood flow, which is then solely derived from the superior vena cava (SVC). In addition to requiring low pulmonary vascular resistance to allow for effective Stage 2 circulation, the surgical reconstruction required to provide a pulmonary blood flow devoid of a ventricular power source must be one that extracts little power or energy. The Hemi-Fontan (HF) operation has been adopted by many surgeons as the preferred procedure to achieve these goals. Figure 1b demonstrates one version of this operation, in which the SVC remains connected to the right atrium, and a homograft patch is placed to redirect flow to the right and left pulmonary arteries through a small pouch or confluence.

Due to the lack of animal models for single ventricle physiology, and the fact that direct clinical measurements are often difficult, the understanding of the impact of the surgical geometries and patient-specific anatomy on important clinical parameters, such as ventricular load, thrombotic risk, or systemic pressures and flows, remains challenging. Computational methods have been used to study patient-specific single ventricle physiology, and predict hemodynamic changes due to virtual surgery (3-8). Using a coupled multi-scale and closed-loop modeling approach, realistic local and global hemodynamic interactions can be mimicked and detailed holistic, physiologic information can be extracted for in-depth analysis to better compare different surgical options.

In this study, we performed virtual HF operation on two patients who had undergone clinical investigation prior to conversion from Stage 1 to Stage 2 circulation. For each patient we investigated the local dynamics of the Hemi-Fontan circulation, and analyzed the global systemic physiology of each under a normal resting state, as well as an "active" state, which mimics voluntary arm and leg movements of the infant with increased heart rate and blood flow.

METHODS

This study utilizes patient-specific computational models to describe various scenarios

after the HF surgery for two single-ventricle patients.   Each computational model contains a 3D domain of the surgical junction, and a 0D domain that describes the rest of the circulatory system.   A total of 4 simulations were performed for this study, encompassing a resting and an active condition for the two patients.

Clinical Data Acquisition

The patients A and B were 5 and 6 months old at the time of surgery, respectively, with body surface areas (BSA) of 0.3 m^2 and 0.34 m^2.   Patients A and B were recruited the Medical University of South Carolina, Charleston SC, and the University of Michigan, Ann Arbor, MI, respectively. The study was approved by the IRB at each institution.   For patient A the MRI was performed 1.5 months prior to surgery, immediately following cardiac catheterization under the same general anesthesia.   For patient B the MRI was performed immediately prior to surgery under the same anesthetic, and cardiac catheterization was performed 3 days prior to the MRI and surgery.   MRI data was obtained using a standardized protocol, including a contrast-enhanced 3-dimensional MR angiogram, following the administration of 0.2 mmol/kg of gadoteridol (Prohance, Bracco Diagnostics, Princeton, New Jersey).   In-plane spatial resolution for the angiogram was 1.0 x 1.0 mm, with slice thickness of 2.0 mm, interpolated to 1.0 mm.

Construction of 3D Surgical Junction Geometries

Based on magnetic resonance imaging data of each patient prior to the Stage 2 surgery, we reconstructed the patient anatomy using commercial software (Mimics, Materialise NV, Leuven, Belgium).   We selected regions of interest in the imaging data, and used a segmentation and region-growing technique (9, 10) to obtain a 3D volume of the relevant vasculature.   The resulting 3D model is a representation of the patient's pre-operative anatomy (Fig. 2b).

Once the pre-operative anatomical models are created, these can be manipulated using the same software (Mimics) in order to generate virtual post-operative scenarios.   We performed the HF virtual surgery by modifying the pre-operative 3D model based on the geometric constraints relating to the organs and vessels surrounding the region.   The post-operative models were created by following the clinical guidelines of the respective procedures, and by the same operator who generated the pre-operative models.   The imaging-based virtual modification of the patient anatomy allows for patient-specific predictions of post-operative geometries.   For example, the post-operative deformation of the SVC is affected by the pulmonary artery geometry at the point of anastomosis.   Using this method, we can produce a predictive HF post-operative 3D geometrical model for each patient (Fig. 2a).   Patient A had a left pulmonary stenosis that was palliated in the virtual surgery, mimicking a realistic clinical scenario.   Both the HF virtual surgeries were performed by an engineer and a pediatric cardiac surgeon working together, and approved by a second surgeon from our research group.

0D Lumped-parameter Network

To model the circulatory system outside of the 3D anatomical region, we use a 0D lumped-parameter network (LPN).   The LPN consists of five main circuit blocks to model the heart, the upper and lower body vasculatures, and the right and left pulmonary vasculatures (Fig. 3).   Two time-varying elastances represent the atrium and ventricle, where two activation functions properly shifted in time model contraction of the two chambers.   The atrio-ventricular and aortic valves are modeled by non-linear diodes allowing for unidirectional flow with resistances proportional to the flow rate.   In the lower body we modeled three organ

systems (kidneys, liver and intestine) and a venous valve in the leg venous block. Corresponding to the outlets of the 3D model, a number of RCR blocks arranged in parallel describe the pulmonary circulation.   Coronary circulation, gravity and respiratory effects are neglected[11].

    We prescribed the pulmonary LPN parameter values using a morphometric tree based impedance approach [12, 13].   The parameters result from a 3D-0D preliminary study utilizing patient-specific preoperative clinical data of the transpulmonary pressure gradient, total pulmonary flow, left-right pulmonary flow split, and the size of each pulmonary branch outlet [13].   The pulmonary vascular resistance can be calculated as:

$$PVR = \frac{P_{PA} - P_{SA}}{Q_{PA}}$$

(1)

where P_{PA}, P_{SA} and Q_{PA} are the mean pulmonary arterial pressure and atrial pressures, and total pulmonary flow, respectively.

    For the systemic LPN parameters, we began with a set of values representing a generic single ventricle subject with BSA=1.8 m^2 [14-16] and used allometric equations to scale the parameters according to the patient's BSA [17].   This resulted in a BSA-adjusted generic LPN model, with resistance and capacitance values indicated as $R_{i\text{-}BSA}$ and $C_{i\text{-}BSA}$ for the ith-block.   We then tuned the LPN to the patient's resting condition using the resistances of the upper and lower body (UBSVR and LBSVR, respectively) calculated by:

$$UBSVR = \frac{P_{SysA} - P_{SA}}{Q_{UBA}} \qquad LBSVR = \frac{P_{SysA} - P_{SA}}{Q_{LBA}}$$

(2)

where P_{SysA}, Q_{UBA}, and Q_{LBA} are the pre-operative (stage 1) clinical measurements of the mean systemic arterial pressure, upper body flow, and lower body flow, respectively.

    While maintaining the proportion of impedances among the different blocks, we modified the resistances of each block (resulting in R_i) such that the clinically measured UBSVR and LBSVR from equations 2 are achieved.   We then calculated the patient-specific compliance C_i of the ith-block using [17, 18]:

$$C_i = C_{i\text{-}BSA} \left(\frac{R_i}{R_{i\text{-}BSA}} \right)^{-4/3}$$

(3)

    Lastly, we manually fine-tuned the parameter values to best match both the mean values and waveform tracings from clinical flow measurements made during resting conditions.   The heart rate for both patient models is set to 120bpm, which is within the range of the measured heart rate in both patients.

    For each patient, we also prescribed a set of LPN parameter values to reflect an "active" condition, which approximates the patient's physiology during voluntary movements of the limbs and increased blood flow.   We chose an "active" state of an infant to parallel an "exercise" state of an older patient capable of exercising.   For the active condition, we assume an increase in heart rate from 120bpm to 160bpm[19], and decreases in PVR and total SVR of 20% and 34%, respectively.   Starting from the patient-specific tuned resting condition LPN model, parameters were systematically tuned, as above, to achieve a set of desired values to model the active state.   The compliances were modified according to the equation:

$$C_{i\text{-}active} = C_i \left(\frac{R_{i\text{-}active}}{R_i} \right)^{-3/4}$$

(4)

where C_i, R_i are the compliances and resistances of the ith-block in the model under resting condition, and $R_{i\text{-}active}$ are the resistances of the ith-block under active condition[20]. All other

model parameters and fluid properties were kept fixed.   In patient A, the PVR and SVR were 0.62 and 4.30 mmHg·s/ml for the resting condition, and 0.49 and 2.87 mmHg·s/ml for the active condition, respectively; for patient B the PVR and SVR were 1.07 and 2.68 mmHg·s/ml for resting and 0.86 and 1.75 mmHg·s/ml for active condition, respectively.

Coupled Multi-scale Simulation & Analysis
        Each of the 3D anatomic models was discretized into an isotropic finite-element mesh with a maximum edge size of 0.03 cm and a total of $9.8 \times 10^5 \sim 1.3 \times 10^6$ linear tetrahedral elements using commercial mesh generation software (MESHSIM, Simmetrix, Inc., NY). These mesh sizes were similar or higher compared to prior studies of corresponding anatomy[21-23].   We coupled the 3D anatomical model to the 0D LPN model to produce a final computational model that described the entire circulation, and numerically solved the coupled system using custom software (Simvascular, www.simtk.org). Neumann boundary conditions were applied at all inlets and outlets of the 3D model using an implicit coupling algorithm described in our previous work[24] in which the 3D domain receives pressure information from the 0D model, and returns flow information to the 0D model, thus completing the two-way coupling between the multi-scale domains.   Flow and pressure in the 0D model were computed from a set of algebraic and ordinary differential equations derived from the LPN circuit, using a 4th order Runge-Kutta method.   Velocity and pressure in the 3D domain were computed using a custom incompressible finite element Navier-Stokes solver, assuming rigid walls and a Newtonian fluid with density of 1.06 g/cm^3 and dynamic viscosity of 0.04 dynes-s/cm^2.   The solver uses a stabilized scheme [25] and outflow stabilization to prevent backflow divergence[26].   The method allows for modular coupling of the 3D and 0D domains without the need for intrusive changes to the finite element solver, and eliminates the small time step stability restriction imposed by explicit coupling methods in previous work. The choice of rigid walls is justified by our recent unpublished work showing little difference in energy loss and pressure levels, though non-negligible differences in wall shear stress (WSS), in rigid vs. deformable simulations.   For each simulation we used a time step size of 1 millisecond for the 3D domain, and 1 microsecond for the 0D domain.   12 cardiac cycles were simulated and the last cycle was used in the analysis.
        Based on the computed 3D velocity field from the simulation, we computed WSS and particle residence time (PRT), which is the time needed for entering particles to exit the 3D HF junction domain.   We also obtained the local hemodynamic power dissipation in the surgical region by integrating the difference between the inlet and outlet energy fluxes of the 3D model, accounting for both the potential and kinetic energy terms[27].   Pressure and flow information at various points in the 0D LPN model were also extracted.   The instantaneous pulmonary power loss is calculated as the sum of the power losses in all of the pulmonary blocks:

$$PW_{pul} = \sum_{outlets}(P_{outlet} - P_{SA}) * Q_{outlet} \tag{5}$$

where P_{outlet}, P_{SA}, and Q_{outlet} are the pressure at each outlet of the 3D model, the atrial pressure, and the volumetric flow through each outlet of the 3D model, respectively.   The pulmonary power loss can then be averaged over the cardiac cycle to obtain a mean value. The ventricular output power is the difference between the work done to the blood by the ventricle, and vice versa, during the ejection and filling phases:

$$PW_{ven} = (\int_{systole} P_{SV} * V_{SV} dt - \int_{diastole} P_{SV} * V_{SV} dt) / T \tag{6}$$

where P_{SV}, V_{SV}, and T are the ventricular pressure, ventricular volume, and the cardiac cycle

period, respectively.

RESULTS

Figures 4a) and 5a) show the volume rendered flow velocity field magnitude (color map) and directions (arrows) in the 3D surgical junction for patients A and B. For both patient models, the incoming flow from the SVC tends to glide along the curve of the confluence floor. In patient A the SVC flow transitions fairly smoothly into the pulmonary arteries. However, in patient B significant swirling is observed, leading to high velocities around the circumference, resulting in a low flow and stagnation region near the center of the confluence section.

Figures 4b) and 5b) show the WSS distribution in the surgical junction for the two patients. In general, WSS is fairly uniformly distributed, with a band of high WSS corresponding to the orientation of the swirling flow in the junction. The spatial pattern of WSS is similar between the resting and active conditions simulated.

Table 1 shows the average values of different parameters extracted from each simulation. The junction power loss associated with the HF in patient B is approximately 3 times of that in patient A, however, the amount of power loss associated with the HF region remained less than 13% of the total power loss in the pulmonary circulation, and less than 2% of the total ventricular output power in all cases.

For both patients, the systemic parameters are significantly affected by changes in the physiological condition, but with different magnitudes. The active state led to increased cardiac output and pulmonary blood flow, and a corresponding increase in SVC pressures in both models. Coupled with an already higher baseline SVC pressure of 15.5 mmHg, Patient B had a much higher SVC pressure in the active condition than Patient A (18.8 vs. 11.7 mmHg, respectively).

Figure 6 shows the ventricular pressure-volume loop and the SVC pressure for all cases. The area inside the pressure-volume loop for the active condition is smaller than that for the resting condition in both patients, indicating that less work is performed during each individual cardiac cycle. However, due to the higher heart rate, the ventricular output power (work divided by time) in the active condition is higher than that in resting.

The mean WSS is higher in the active state compared to the resting state (82% and 75% higher, for patients A and B, respectively). The mean PRT, on the other hand, is higher in the resting state compared to the active state (50% and 41% higher, for patients A and B, respectively).

DISCUSSION

This study demonstrates the potential of multi-scale techniques to study the hemodynamics and physiology of Stage 2 circulation with the HF procedure in patients with single ventricle circulation. A coupled closed-loop multi-scale modeling approach was used to mimic realistic post-operative scenarios in two patients based on pre-operative clinical data. This method allowed assessment of both local dynamic and global physiologic parameters in a patient-specific manner, and demonstrated that even with the same type of operation, differences in hemodynamic outcomes can occur. Moreover, these differences can be accentuated by virtually 'stressing' the circulation by changing parameters to mimic physiologic conditions in an active state. By varying modeling parameters, such as heart rate and systemic/pulmonary vascular resistances, this methodology provides important insights into the effects of changes in physiologic condition on the Stage 2 circulation.

The power loss results are in the same range as reported by previous modeling studies of the HF anatomy(22, 23). The simulation results show significant differences in the 3D

velocity patterns in the surgical domains in the two different patients, leading to visible variations in power loss.   Patient B exhibited three times higher power loss due to higher degrees of flow disturbances and flow rates.   However, relative to the global systemic powers, such as the pulmonary circulation power loss and ventricular power, the power loss in the surgical domain is small and may not have a large influence on the overall circulation. The observed differences in global flow and pressures, for example cardiac output and SVC pressure, between Patient A and B were primarily due to differences in patient-specific physiologic parameters such as pulmonary vascular resistance. These results therefore imply that further refinement of the HF operation and improvements in the surgical junction power loss is likely to have minimal impact on the overall immediate post-operative circulation and physiology in terms of pressure and flow, at least during resting and regular active conditions.

Nevertheless, refinement of the HF operation may consider the optimization of minimizing thrombotic risk.   Results from computational simulations such as PRT and WSS can contribute to assessing the relative thrombotic risks between the different cases.   The lower PRT during the active condition may be beneficial for reducing thrombotic risk. However, the higher WSS during the active state may pose risks of platelet activation.   The peaking levels of WSS observed in the scenarios investigated are within the range where shear-induced platelet activation is possible (28).

The observation that the active condition increased the surgical junction power loss can be explained by considering the junction as a non-linear resistance with a value proportional to the square of the flow rate(29).   Auto-regulation mechanisms also act to increase vessel diameters during an active state, decreasing vascular resistance in response to increased flow (30).   This was included in the models by the chosen changes in PVR and SVR.   For these reasons, with increasing cardiac output, the surgical junction power loss increases at a faster rate than systemic power losses.   The surgical junction power loss relative to systemic losses thus will become more significant at higher cardiac output.   The power loss difference between the two HF models could become important and have more tangible effects on systemic parameters with more extreme physiological conditions such as strenuous activity (27).   As noted in the active condition simulation, the increase in SVC pressure for patient B is more exaggerated than patient A, with pressures reaching 19 mmHg. This has important clinical ramifications.   While most patients would tolerate an SVC pressure up to 15 to 16 mmHg, at 19 mmHg it is likely that patient B would exhibit clinical signs of SVC syndrome or superior venous hypertension, with facial swelling, headache, and orbital edema, based on prior clinical experience.

This study demonstrates that, in the Stage 2 circulation, while differences in local dynamics and power loss can exist with the HF procedure between different patients, the impact on the global circulation is small compared to those of pulmonary power losses and ventricular power.   In addition, the application of a multi-scale model was shown to accurately capture single ventricle patient physiology, incorporating clinical data for customized virtual planning and prediction of the stage 2 procedure, as well as utility in modeling systemic behaviors under different physiological states. Results show that differences in hemodynamic factors in different patient geometries can be accentuated by higher stress physiologic conditions, such as increased activity.   The unique contributions of this study include the examination of different physiological conditions using a closed-loop multi-scale model, and the examination of parameters relevant to both thrombotic risk and energy loss.   The results of this study provide an evaluation on the relative importance of various considerations for the clinical procedure design for the stage 2 surgery.

Thorough analyses on a sufficient population size are required in order to warrant changes in clinical procedures based on virtual simulation results.   Future studies will apply

these simulation methods to a larger number of patients, and examine additional parameters such as ventricular function, and compare different surgical options for the Stage 2 surgery. Limitations of this study include the need for further validation against both clinical and in vitro data, use of rigid walls, and a lack of clinical data to precisely model changes in PVR and other parameters from the pre- to post-operative state.

ACKNOWLEDGEMENTS

CONFLICT OF INTEREST STATEMENT

There are no conflict of interest associated with this work.

REFERENCES

1.   Gale AW, Danielson GK, McGoon DC, Wallace RB, Mair DD. (1980) Fontan procedure for tricuspid atresia. Circulation 62:91-96.
2.   Bardo DM, Frankel DG, Applegate KE, Murphy DJ, Saneto RP. (2001) Hypoplastic left heart syndrome. Radiographics 21:705-717.
3.   Marsden AL, Reddy VM, Shadden SC, Chan FP, Taylor CA, Feinstein JA. (2010) A new multiparameter approach to computational simulation for Fontan assessment and redesign. Congenit Heart Dis 5:104-117.
4.   Vignon-Clementel IE, Marsden AL, Feinstein JA. (2010) A primer on computational simulation in congenital heart disease for the clinician. Progress in Pediatric Cardiology 30:3-13.
5.   Pekkan K, Whited B, Kanter K, et al. (2008) Patient-specific surgical planning and hemodynamic computational fluid dynamics optimization through free-form haptic anatomy editing tool (SURGEM). Med Biol Eng Comput 46:1139-1152.
6.   Marsden AL, Bernstein AJ, Reddy VM, et al. (2009) Evaluation of a novel Y-shaped extracardiac Fontan baffle using computational fluid dynamics. J Thorac Cardiovasc Surg 137:394-403.e392.
7.   Sundareswaran KS, de Zélicourt D, Sharma S, et al. (2009) Correction of Pulmonary Arteriovenous Malformation Using Image-Based Surgical Planning. JACC: Cardiovascular Imaging 2:1024-1030.
8.   de Zélicourt DA, Haggerty CM, Sundareswaran KS, et al. (2011) Individualized computer-based surgical planning to address pulmonary arteriovenous malformations in patients with a single ventricle with an interrupted inferior vena cava and azygous continuation. The Journal of Thoracic and Cardiovascular Surgery 141:1170-1177.
9.   Armillotta A, Bonhoeffer P, Dubini G, et al. (2007) Use of rapid prototyping models in the planning of percutaneous pulmonary valved stent implantation. Proceedings of the Institution of Mechanical Engineers, Part H: Journal of Engineering in Medicine 221:407-416.
10.   Schievano S, Migliavacca F, Coats L, et al. (2007) Percutaneous pulmonary valve implantation based on rapid prototyping of right ventricular outflow tract and pulmonary trunk from MR data. Radiology 242:490-497.

11.   Migliavacca F, Pennati G, Dubini G, et al. (2001) Modeling of the Norwood circulation: effects of shunt size, vascular resistances, and heart rate. American Journal of Physiology-Heart and Circulatory Physiology 280:H2076-H2086.

12.   Spilker RL, Feinstein JA, Parker DW, Reddy VM, Taylor CA. (2007) Morphometry-based impedance boundary conditions for patient-specific modeling of blood flow in pulmonary arteries. Ann Biomed Eng 35:546-559.

13.   Troianowski G, Taylor CA, Feinstein JA, Vignon-Clementel IE. (2011) Three-dimensional simulations in Glenn patients: clinically based boundary conditions, hemodynamic results and sensitivity to input data. J Biomech Eng 133:111006.

14.   Noordergraaf A, Verdouw D, Boom HB. (1963) The use of an analog computer in a circulation model. Prog Cardiovasc Dis 5:419-439.

15.   Snyder MF, Rideout VC, Hillestad RJ. (1968) Computer modeling of the human systemic arterial tree. J Biomech 1:341-353.

16.   Snyder MF, Rideout VC. (1969) Computer simulation studies of the venous circulation. IEEE Trans Biomed Eng 16:325-334.

17.   Pennati G, Fumero R. (2000) Scaling Approach to Study the Changes Through the Gestation of Human Fetal Cardiac and Circulatory Behaviors. Annals of Biomedical Engineering 28:442-452.

18.   Baretta A, Corsini C, Yang W, et al. (2011) Virtual surgeries in patients with congenital heart disease: a multi-scale modelling test case. Philosophical Transactions of the Royal Society A: Mathematical, Physical and Engineering Sciences 369:4316-4330.

19.   Berg KM, Berg WK, Graham FK. (1971) INFANT HEART RATE RESPONSE AS A FUNCTION OF STIMULUS AND STATE. Psychophysiology 8:30-44.

20.   Baretta A, Corsini C, Marsden AL, et al. (2012) Respiratory effects on hemodynamics in patient-specific CFD models of the Fontan circulation under exercise conditions. European Journal of Mechanics-B/Fluids.

21.   Yang W, Vignon-Clementel IE, Troianowski G, Reddy VM, Feinstein JA, Marsden AL. (2011) Hepatic blood flow distribution and performance in conventional and novel Y-graft Fontan geometries: A case series computational fluid dynamics study. J Thorac Cardiovasc Surg.

22.   Pekkan K, Dasi LP, de Zélicourt D, et al. (2009) Hemodynamic performance of stage-2 univentricular reconstruction: Glenn vs. hemi-Fontan templates. Ann Biomed Eng 37:50-63.

23.   Bove EL, de Leval MR, Migliavacca F, Guadagni G, Dubini G. (2003) Computational fluid dynamics in the evaluation of hemodynamic performance of cavopulmonary connections after the Norwood procedure for hypoplastic left heart syndrome. J Thorac Cardiovasc Surg 126:1040-1047.

24.   Esmaily Moghadam M, Bazilevs Y, Hsia TY, Vignon-Clementel IE, Marsden AL. (2011) A comparison of outlet boundary treatments for prevention of backflow divergence with relevance to blood flow simulations. Computational Mechanics:1-15.

25.   Taylor CA, Hughes TJR, Zarins CK. (1998) Finite element modeling of blood flow in arteries. Computer Methods in Applied Mechanics and Engineering 158:155 - 196.

26.   Esmaily Moghadam M, Migliavacca F, Vignon-Clementel IE, Hsia T-Y, Marsden AL. Optimization of shunt placement for the Norwood surgery using multi-domain modeling. J Biomech Eng.

27.   Marsden AL, Vignon-Clementel IE, Chan FP, Feinstein JA, Taylor CA. (2007) Effects of exercise and respiration on hemodynamic efficiency in CFD simulations of the total cavopulmonary connection. Ann Biomed Eng 35:250-263.

28.   Brown CH, Leverett LB, Lewis CW, Alfrey CP, Hellums JD. (1975) Morphological, biochemical, and functional changes in human platelets subjected to shear stress. J Lab Clin Med 86:462-471.

29.   Whitehead KK, Pekkan K, Kitajima HD, Paridon SM, Yoganathan AP, Fogel MA. (2007) Nonlinear power loss during exercise in single-ventricle patients after the Fontan: insights from

computational fluid dynamics. Circulation 116:I165-I171.

30.   Goto C, Higashi Y, Kimura M, et al. (2003) Effect of different intensities of exercise on endothelium-dependent vasodilation in humans: role of endothelium-dependent nitric oxide and oxidative stress. Circulation 108:530-535.

TABLE AND FIGURE CAPTIONS

Table 1.   Mean Values of Simulated Results.   Pressures and flows are as labeled in figure 3.

Figure 1.   Single Ventricle Palliation Surgical Procedures: a) Stage 1, b) Stage 2 Hemi-Fontan.   (Figure 1a republished with kind permission from Springer Science and Business Media, originally published in Pediatric Radiology 2010;40, Cardiovascular magnetic resonance imaging of hypoplastic left heart syndrome in children, Dillman JR et al, p264, figure 4, illustration by Anne Phillips, University of Michigan Health System, Department of Radiology Media Services.   Figure 1b produced by Carolyn Nowak, University of Michigan Health System, Department of Radiology Media Services.)

Figure 2.   a)   Work Flow of Model Construction From Imaging Data, and Virtual Hemi-Fontan Surgery.   b)   Pre-operative 3D Anatomical Models of Patients A & B

Figure 3.   The 0D Lumped-parameter Network Model Coupled to the 3D Anatomical Model.

Figure 4.   Time-averaged 3D Domain Simulation Results for Patient A.   a) Volume-rendered velocity magnitude (color map) and directions (arrows), b) Wall shear stress distribution.

Figure 5.   Time-averaged 3D Domain Simulation Results for Patient B.   a) Volume-rendered velocity magnitude (color map) and directions (arrows), b) Wall shear stress distribution.

Figure 6.   Simulated Results of Ventricular Pressure-Volume Loop and SVC Pressure for a) Patient A, and b) Patient B.

Table 1.

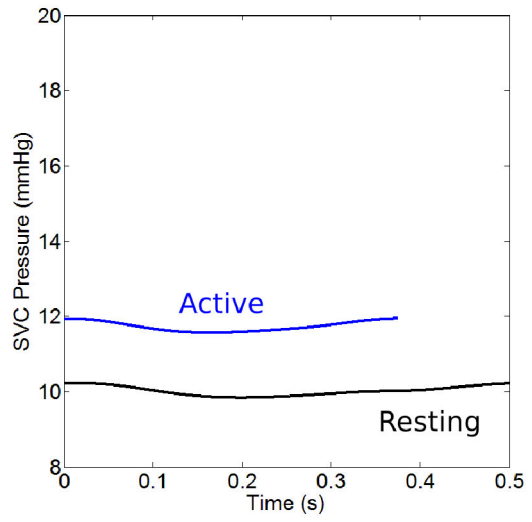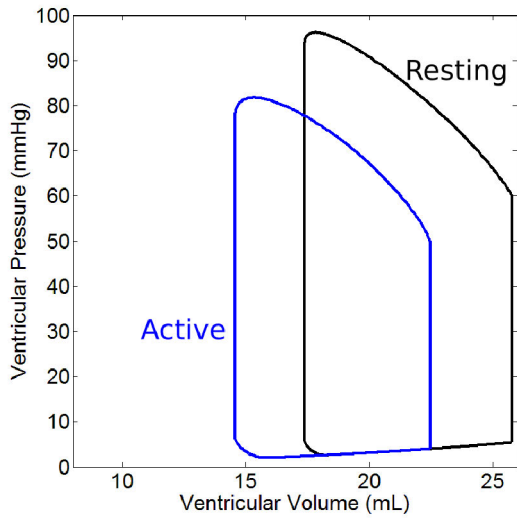|	Patient A		Patient B	
	Resting	Active	Resting	Active
Q_{AO} (mL/s)	16.8	21.0	19.2	24.6
Q_{PV} (mL/s)	8.2	12.7	11.3	16.4
Q_{RPV} / Q_{PV}	0.54	0.53	0.63	0.62
Q_{PV} / Q_{AO}	0.49	0.60	0.59	0.67
P_{SA} (mmHg)	4.6	4.8	2.4	3.0
P_{SVC} (mmHg)	10.0	11.7	15.4	18.8
P_{AO} (mmHg)	74.9	62.0	53.1	46.3
Wall Shear Stress (dynes/cm²)	10.62	19.34	20.64	36.05
Particle Residence Time (s)	0.27	0.18	0.31	0.22
Junction Power Loss (mW)	0.33	1.01	1.26	3.79
Pulmonary Power Loss (mW)	5.6	10.7	18.2	30.7
Ventricular Power (mW)	193	209	168	193
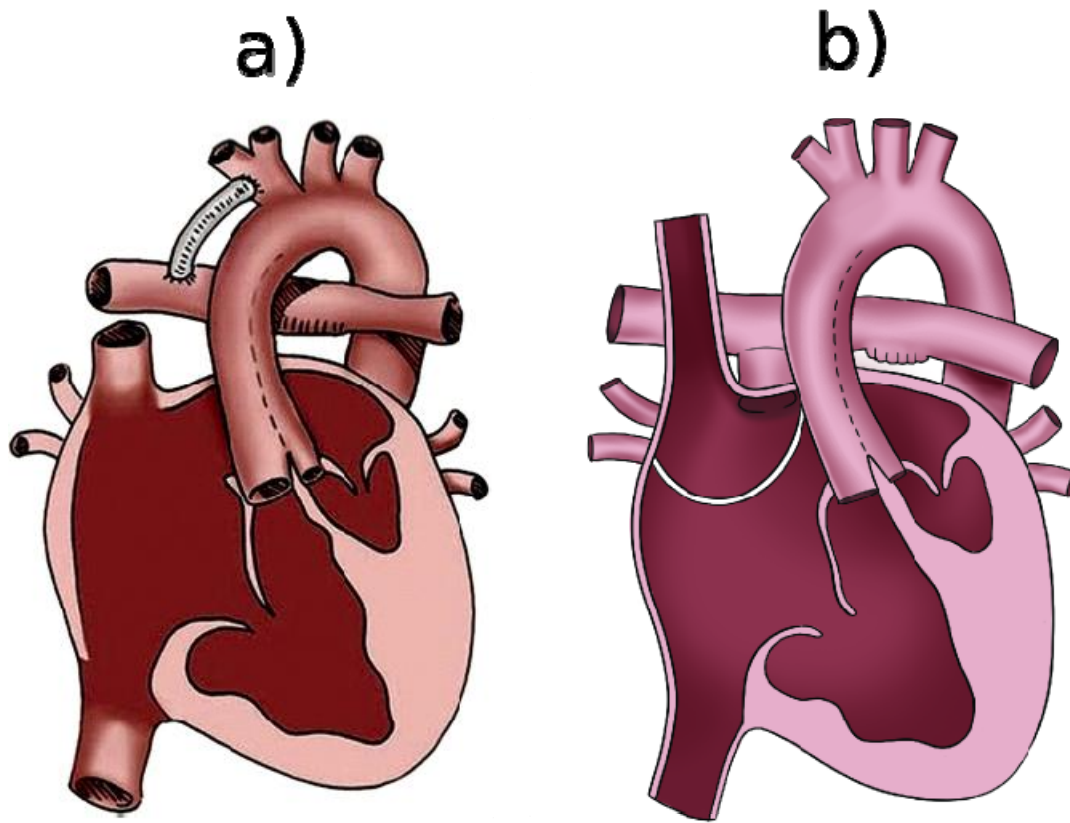
Figure 1.
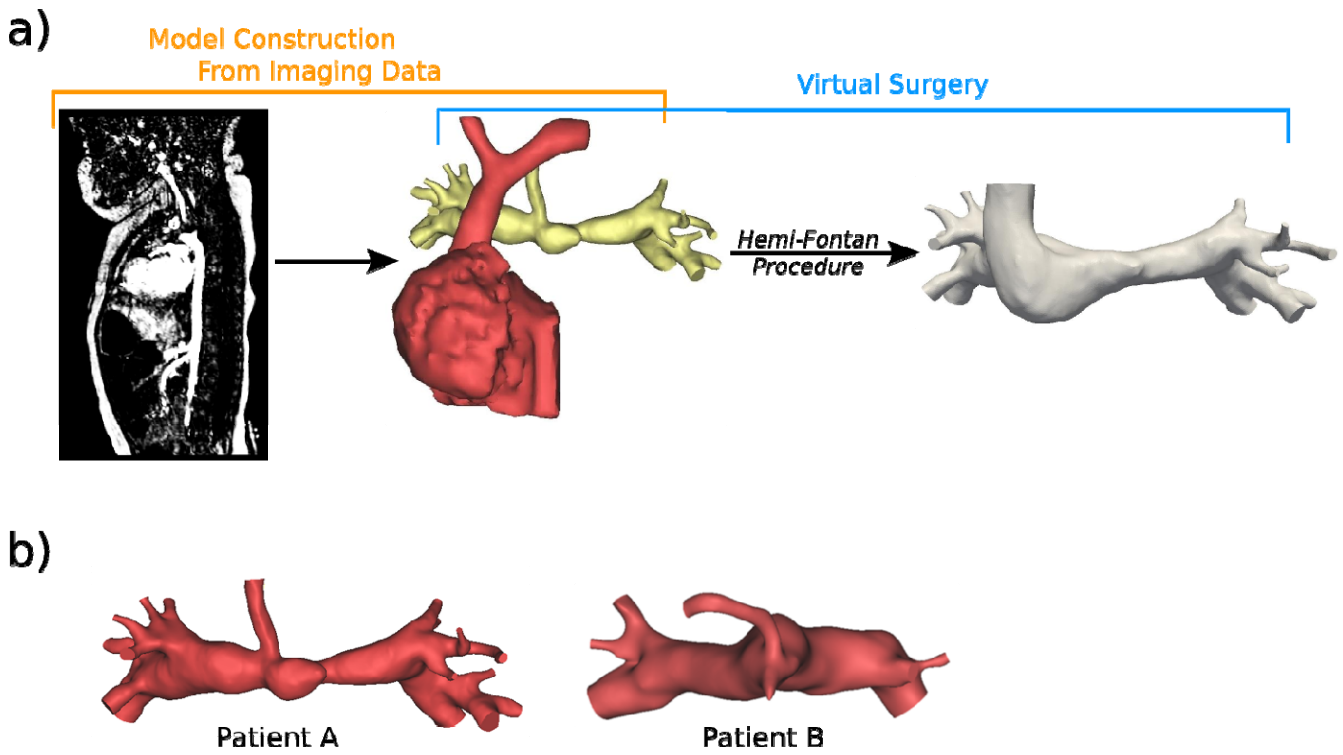
Figure 2.
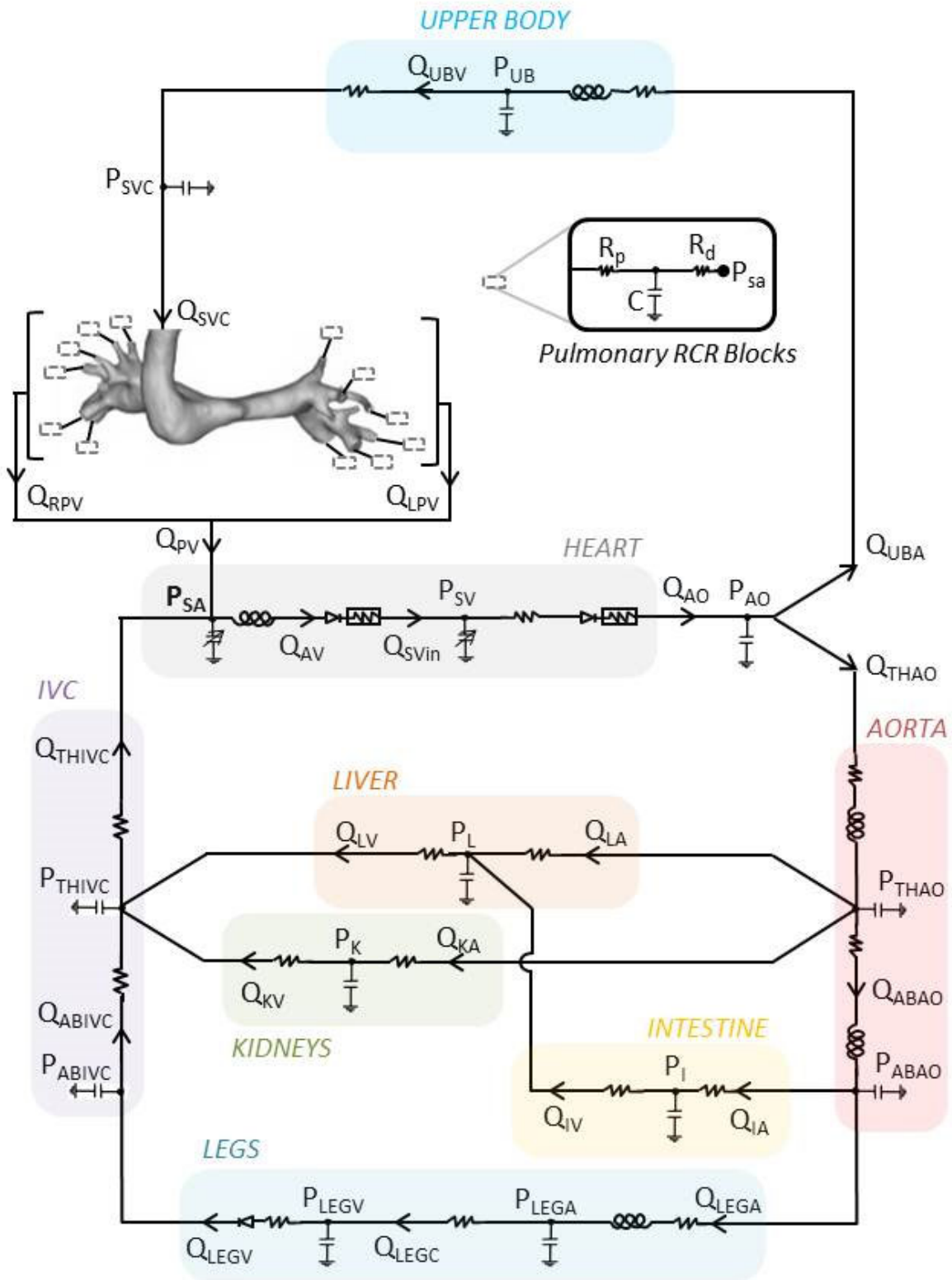
Figure 3.

Figure 4.

Figure 5.

Figure 6.